inorganics

MDPI

Article

Hybrid Siloxane Materials Based on a Mutually Reactive Epoxy–Amine System: Synthesis, Structure, and Thermal Stability Investigations

Maria Emiliana Fortună [1], Maria Ignat [1,2,*], Niţă Tudorachi [1], Elena Ungureanu [3], Răzvan Rotaru [1] and Valeria Harabagiu [1]

[1] "Petru Poni" Institute of Macromolecular Chemistry, Department of Inorganic Polymers, 41A Grigore Ghica Voda Alley, 700487 Iasi, Romania; rotaru.razvan@icmpp.ro (R.R.); hvaleria@icmpp.ro (V.H.)
[2] Faculty of Chemistry, "Alexandru Ioan Cuza" University, 11 Bd. Carol I, 700506 Iasi, Romania
[3] Department of Exact Sciences, "Ion Ionescu de la Brad" Iasi University of Life Sciences, 3 Mihail Sadoveanu Alley, 700490 Iasi, Romania; elena.ungureanu@iuls.ro
* Correspondence: ignat.maria@icmpp.ro or maria.ignat@uaic.ro; Tel.: +40-746505227

Abstract: Hybrid siloxane materials based on a mutually reactive epoxy–amine system are organic-inorganic hybrid materials synthesized via the sol–gel reaction of siloxane precursors, followed by the polymerization of organo-functionalized oligosiloxanes. Therefore, using a new hybrid system as the reaction product resulting from the reaction between 1,3-bis(3-glycidoxypropyl)-l, 1,3,3-tetramethyldisiloxane—$C_{16}H_{34}O_5Si_2$—(gp-DS) and p-phenylenediamine—$C_6H_4(NH_2)_2$—(PPD), an aromatic diamine, was obtained. The chemical structure of the synthesized hybrid siloxane material was confirmed via Fourier Transform Infra-Red (FTIR) spectroscopy, mass spectrometry (MS), and ^{1}H-NMR spectroscopy. The morphology and surface chemical composition was highlighted via scanning electron microscopy (SEM) equipped with an EDX elemental analysis system. Further, the thermal stabilities of the prepared hybrid siloxane and its precursors have been investigated via thermogravimetric analysis (TGA), proving the modification of epoxy-functional disiloxanes with a paraphenylenediamine reagent that made it possible to produce hybrid siloxane materials with very good thermal stabilities and dual weak hydrophilic/hydrophobic surfaces.

Keywords: p-phenylenediamine (PPD); 1,1,3,3 tetramethyldisiloxane (DS); hybrid materials; thermal stability

Citation: Fortună, M.E.; Ignat, M.; Tudorachi, N.; Ungureanu, E.; Rotaru, R.; Harabagiu, V. Hybrid Siloxane Materials Based on a Mutually Reactive Epoxy–Amine System: Synthesis, Structure, and Thermal Stability Investigations. *Inorganics* **2024**, *12*, 118. https://doi.org/10.3390/inorganics12040118

Academic Editor: Francis Verpoort

Received: 14 March 2024
Revised: 11 April 2024
Accepted: 15 April 2024
Published: 17 April 2024

1. Introduction

Siloxanes contain -Si–O–Si-O- inorganic backbones and organic substituents linked to silicon atoms and can play the role of building blocks for hybrids and organic–inorganic composites. However, the properties of these hybrid materials mainly depend on the nature of organic substituents (aliphatic, aromatic, organo-, or silico-functional groups) bonded to silicon atoms. Usually, placing reactive groups (epoxy, alkoxy, hydroxyl, amino groups, etc.) in their molecular structure allows for yielding products of unique physicochemical properties, which can be used as surfactants, biomaterials, personal care products, membranes, adhesives, electrical insulators, etc. [1]. Recently, dynamic siloxane materials and their application in energy, electronic, and smart optical devices; antifouling and anti-biofouling surfaces; actuators; and advanced manufacturing have been reviewed [2]. On the other hand, epoxy resins are of great economic importance based on their specific properties, such as good mechanical properties and dimensional stability, wetting ability, low curing shrinkage, and chemical stability [3,4]. The preparation of these materials starts from different types of epoxides, which are cured with amine with different crosslinkers such as aliphatic/aromatic amines, phenols, thiols, acids, etc., in the presence of different catalysts

or activators [5,6]. Quite recently, crosslinkers based on renewable resources were also proposed [7,8]. Despite their useful properties, their uses are not as high as expected because they are brittle materials of low-impact strength [9,10]. To overcome these drawbacks epoxy-resins are combined with different, more flexible polymers. Thus, siloxane-modified epoxy resins were prepared and tested as anticorrosive coatings or thermally resistant materials [11–13]. Moreover, it was found that epoxy functionality can improve the adherence of adhesives and coatings through reaction with acrylic, polyurethane, or amine-hardeners. Moreover, the grafting of the epoxy group onto siloxanes has a wide range of applications: materials such as sealants, lubricants, surfactants, rubbers, coatings, and adhesives [14], owing to the excellent mechanical, electrical, and adhesive properties of the resulting epoxy resins. For this reason, these materials are used as high-performance thermosetting materials in various industrial fields. One of the ways to improve its effectiveness in pressure-sensitive adhesive application is to increase the glass transition temperatures (T_g) of siloxanes. As a consequence, the amino-functionalization of siloxanes was found to be a great solution for assessing a higher glass transition temperature compared to methyl-functionalization [15].

In addition, widely used epoxy hardeners, as well as aliphatic or aromatic amines, are well-known curing agents. Thus, to fabricate a wide class of thermosetting organic polymers based on the epoxy–amine system, polyfunctional amines are usually used as the most popular curing agents [16,17], showing several epoxy−amine curing reaction mechanisms. Among these mechanisms, direct amine addition to the epoxy groups is considered a very useful method for crosslinking epoxy resins, the reaction being used for the production of hybrid materials by making use of epoxy-functional siloxanes. Therefore, a derivative of the aromatic amine (aniline), such as p-phenylenediamine (PPD), could be considered a viable option for the role of curing agent in such reactions. This organic compound has been found to have applications in organic and coordination chemistry, as a precursor to certain polymers, plastics, and fibers; as a photographic developing agent; and as a histological stain for some lipids [18], but there are still many investigations focusing on finding its new uses.

Broadly speaking, epoxy–siloxane amine composites could be useful in coatings where the good weathering performance of siloxanes is desirable. However, the possibilities for using the direct-amine-addition-based synthesis to produce hybrid materials have not been well explored [19]. To the best of our knowledge, the reaction mechanism, material structure, and thermal properties have been the subject of extensive research reported in the literature [4,20]; however, more investigations are still necessary to clarify every detail of the epoxy−amine curing reaction.

Thus, the present research study is focused on the synthesis procedure of modified diepoxy-functional disiloxanes, using $C_6H_4(NH_2)_2$ (PPD), as a curing agent, and $C_{16}H_{34}O_5Si_2$ (gp-DS). Prior to this reaction, the hydrosilation reaction of allyl glycidyl ether with 1,1,3,3-tetramethyldisiloxane was performed in the presence of a Karsted catalyst [21]. Thereby, the results reported in this study are aimed at finding the thermal stability of the prepared hybrid p-Phenylenediamine-disiloxane—$C_{22}H_{42}O_5Si_2$ N_2—(DS-PPD) assigned to the reactive epoxy and amino groups grafted.

2. Results and Discussion

2.1. Structural Analysis

The chemical structure of the DS-PPD conjugate, compared to its precursors, was confirmed by applying infrared spectroscopy (FT-IR) analysis. Thus, Figure 1 shows the comparative FT-IR spectra of the DS-PPD (1/0.5) sample with those of the PPD and gp-DS precursors. It is observed that the spectrum of the gp-DS sample shows no Si-H bond stretching at 2160 cm^{-1}, proving the complete hydrosilation reaction recorded for its synthesis. As one may see in Figure 1, the DS-PPD compound reveals the specific bands characteristic of both precursors, but these bands are more or less shifted compared with the starting compounds. The characteristic = C-H stretches of the aromatic ring found

at 3196 cm^{-1} and 3007 cm^{-1} in the PPD spectrum were blue-shifted at 3213 cm^{-1} and 3035 cm^{-1} in the IR spectrum of DS-PPD, meaning that the C-H bond becomes polarized upon interaction; thus, the positive charge on the H and the negative charge on the C are increased and the C-H bond is strengthened. On the other hand, quite important shifts to higher frequencies of N–H stretches of amines (3447 cm^{-1} and 3343 cm^{-1}) and N–H bending vibrations of primary amines (1674 cm^{-1}) are also observed compared to the same characteristic bands found in PPD spectrum (3406 cm^{-1}, 3375 cm^{-1}, 1628 cm^{-1}), indicating a strengthening of the N-H bond. Moreover, the epoxy characteristic band of gp-DS was detected at 910 cm^{-1} and disappeared in the FT-IR spectrum of DS-PPD, indicating the epoxy-ring opening in the synthesis reaction of the hybrid siloxane material [22].

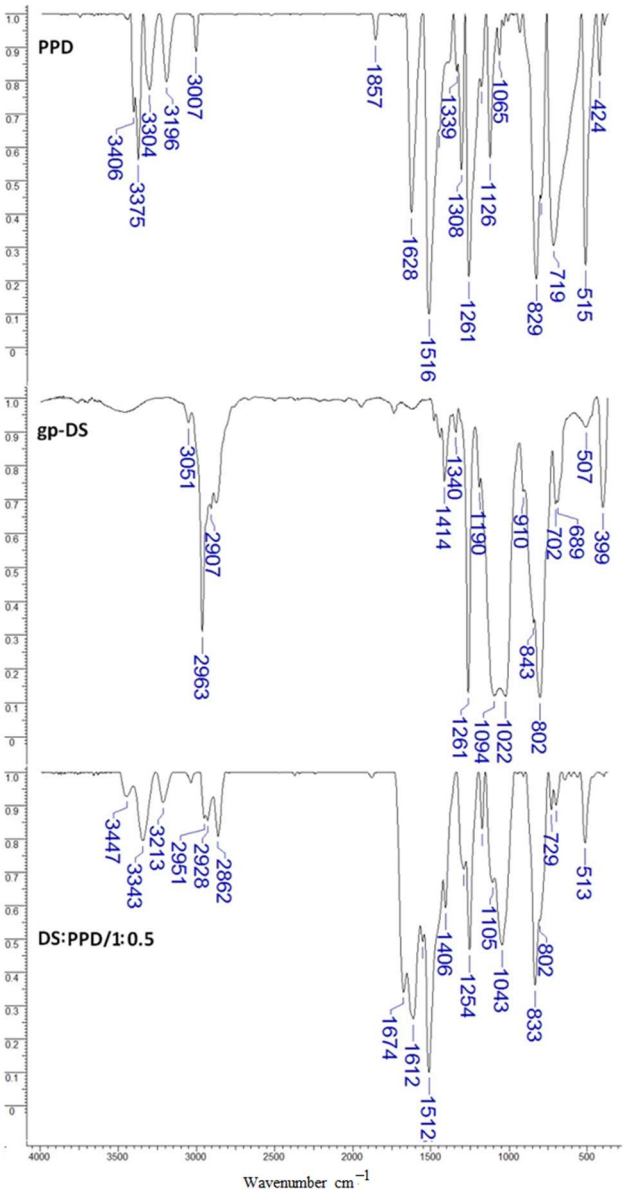

Figure 1. FT-IR spectra of the PPD, gp-DS, and DS-PPD samples.

Further, the registered proton NMR spectra confirmed the structures of the prepared gp-DS precursor and DS-PPD hybrid siloxane sample, and they are shown in Figure 2a,b. As observed, the Si–H resonance at δ = 4.7 ppm is almost absent in the spectrum of the gp-DS sample. In addition, the peaks at δ = 0.5 ppm, 1.6 ppm, and 3.4 ppm are the resonance peaks assigned to the propyl group attached to the silicon atom, while those found at δ = 2.5 ppm, 2.7 ppm, and 3.1 ppm represent the resonance peaks of the epoxide group.

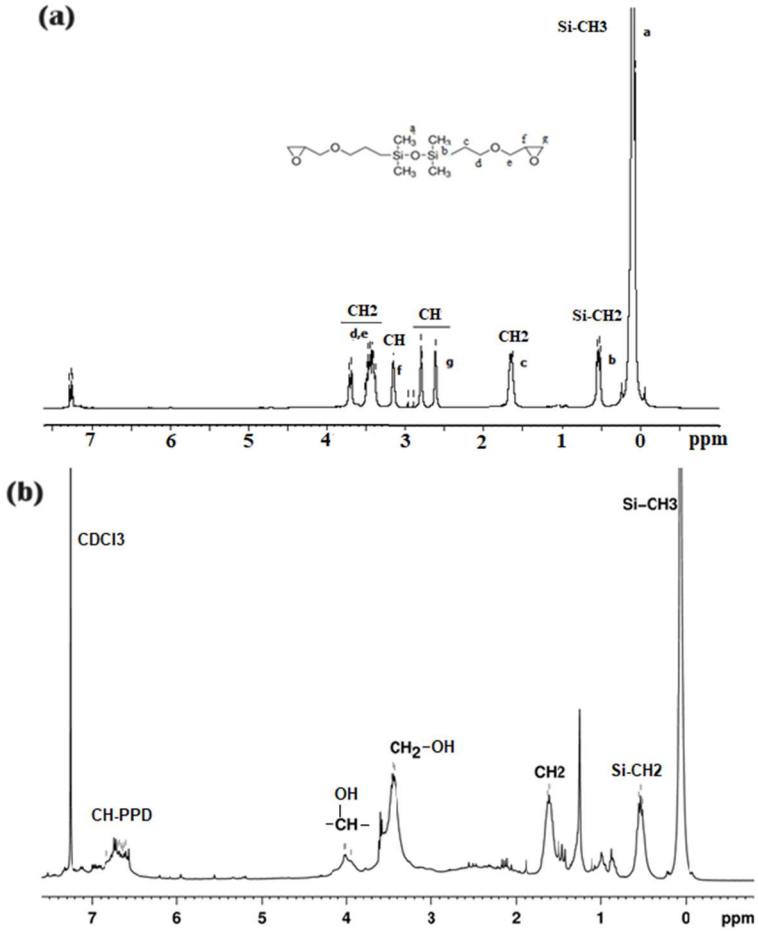

Figure 2. The ^{1}H-NMR spectra of (**a**) gp-DS (the lowercase letters indicate protons with assigned peaks in the spectrum) and (**b**) DS-PPD soluble fraction samples recorded at 400 MHz in $CDCl_3$.

The reaction occurring between PPD and gp-DS reactants was confirmed by the NMR spectrum of the resulting gp-PPD product, where the signals of epoxy-ring protons of gp-DS are no longer visible and a new peak located around 4.01 ppm attributed to the newly formed CH(OH) group appeared. Moreover, aromatic protons of PPD linked to the siloxane moiety are visible as a multiplet in the region 6.61–6.83 ppm.

2.2. Morphology and Qualitative Composition of DS-PPD Conjugate

The surface morphology of the DS-PPD sample and its qualitative composition was determined via scanning electron microscopy (SEM) coupled with energy dispersive X-ray analysis (EDX) (Figure 3). A rough surface with a non-uniform inner porosity is evidenced in the SEM image (Figure 3a). The EDX elemental analysis was performed in triplicate to determine the weight%/atomic% for each identified element. It was expected that discrepancies between experimentally determined percentages and theoretically calculated ones would appear due to EDX surface analysis not being in the depth of the sample. However, the determined weight percentage values are not so far from the calculated ones, considering that hydrogen could not be quantified via EDX analysis. The registered EDX spectrum for the DS-PPD (1/0.5) sample is shown in Figure 3b, revealing the main peaks of C, N, O, and Si elements coming from both PPD and DS reactants. The presence of the high peak at the approximately 1.75 keV characteristic of the Si atom was assigned to the siloxane fragment, as reported by researchers elsewhere [23].

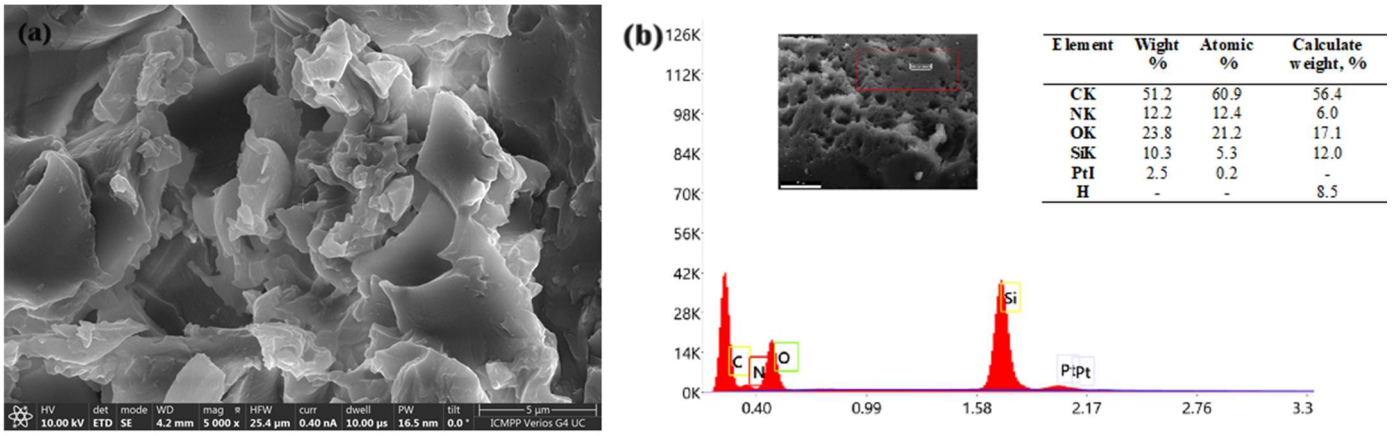

Figure 3. (**a**) The SEM image of the DS-PPD prepared material and (**b**) energy-dispersive X-ray analysis (EDX) spectrum of the purified DS-PPD (1/0.5) sample.

2.3. Thermal Stability Study

The thermal stabilities of crosslinked siloxane-p-phenylenediamine (DS-PPD 1/0.5), gp-DS, and PPD reactants were investigated via thermogravimetric analysis. Consequently, the registered TG (Thermogravimetric) and DTG (Derivative Thermogravimetric) curves recorded with a 10 °C min^{-1} heating rate, in a nitrogen atmosphere, are shown in Figure 4, while Table 1 provides the thermal parameters for all investigated samples. Thus, analyzing the obtained results, we can conclude that the thermal behavior of the DS-PPD (1/0.5), gp-DS, and PPD materials can be assessed in terms of weight percentage loss by monitoring the sample weight evolution during the heating process in the temperature range of 20–700 °C.

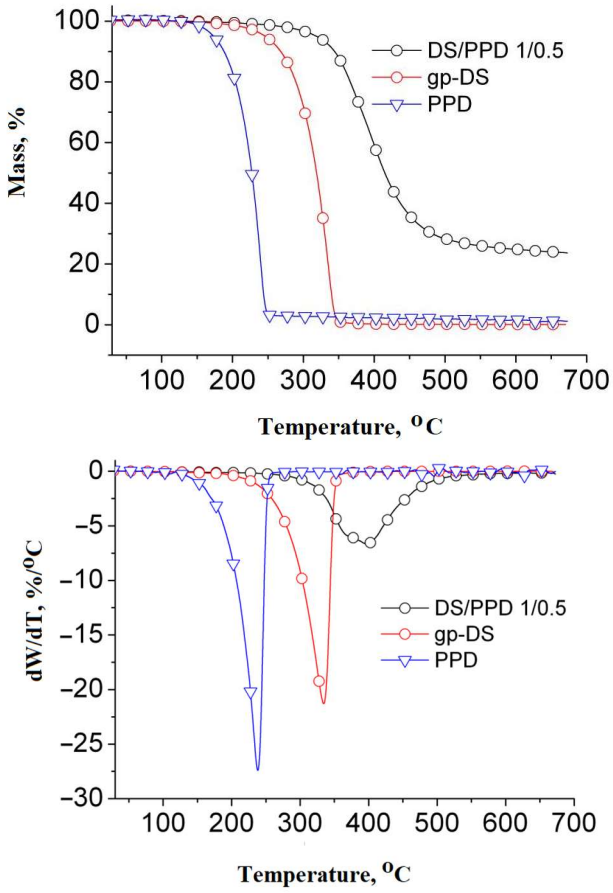

Figure 4. TG and DTG curves for DS-PPD (1/0.5), gp-DS, and PPD samples.

Table 1. The main thermal parameters characteristic to the DS-PPD (1/0.5), gp-DS, and PPD samples.

Sample	Heating Rate °C/min	Degradation Stage	T_{onset} DTG °C	T_{peak} °C	*W* %	T_{10} °C	T_{20} °C	*GS* °C
DS/PPD (1/0.5)	10	I residue	322	398	76.35 23.65	344	366	390
gp-DS	10	I residue	287	337	99.88 0.12	270	292	-
PPD	10	I residue	204	237	98.82 1.18	187	203	-

T_{onset}—the temperature at which the thermal degradation starts; T_{peak}—the temperature at which the degradation rate is maximum; T_{10}, T_{20},—the temperatures corresponding to 10% and 20% mass losses; *GS*—the temperature at which the maximum quantity of gasses was released (determined from Gram–Schmidt curves using Proteus software); *W*—mass losses up to 700 °C.

As observed, all TG and DTG curves show a single thermal degradation process located at different temperatures for each investigated sample. It was found that gp-DS and PPD were completely decomposed into volatiles in the temperature range of 250–350 °C. As observed, the TG curves of PPD and gp-DS show a sudden and rapid decrease in the mass loss with T_{onset} located at 204 °C and 287 °C. On the other hand, the crosslinked DS-PPD presents a wide thermal degradation process that starts at a higher temperature (T_{onset} = 322 °C) and occurs at a lower speed. Whereas the gp-DS sample recorded a mass loss of 99.88% with T_{peak} = 337 °C, the PPD sample showed a mass loss of 98.82%, with a T_{peak} value at a lower temperature of 237 °C. In the case of the DS-PPD prepared hybrid material, the resulting character of the combination of the two components reveals an improvement in thermal stability, as observed, with the T_{peak} recorded at a higher temperature suggesting that the product is crosslinked. The mass loss starts at 76.35% and continues at a higher temperature up to 398 °C, at which point the thermal decomposition rate is maximum. Considering the mass losses of 10% and 20% that occur at a specific temperature, the T_{10} and T_{20} temperature values (Table 1) can assess the thermal stability of the examined samples. Thus, as the DS-PPD synthesized hybrid material exhibits the highest values of these thermal parameters (T_{10} = 344 °C and T_{20} = 366 °C) compared to the reactants used for its synthesis, gp-DS (T_{10} = 270 °C and T_{20} = 292 °C) and PPD (T_{10} = 187 °C and T_{20} = 203 °C) samples, an improved thermal stability is demonstrated. Further, considering the above-presented data, the thermal stability of the investigated compounds can be arranged in a series as follows: PPD < gp-DS < DS-PPD.

In addition, the crosslinked hybrid material, the DS-PPD (1/0.5) sample, was subjected to further thermal investigation using advanced thermogravimetric analysis, namely TGA/FT-IR/MS. Thus, to monitor the gas emission via thermal decomposition, the temperature-dependent FT-IR 3D spectrum of the DS-PPD (1/0.5) solid sample was registered in the temperature range of 30–650 °C. The used analysis technique allowed for the simultaneous recording of the sample weight decrease with the registrations of the IR-absorbance and MS spectra of the gas emissions. Thus, Figure 5a shows the FT-IR 3D spectrum recorded over the whole temperature range, while Figure 5b reveals the FT-IR 2D spectrum of the evolved gasses during the thermal degradation of the DS-PPD (1/0.5) sample, recorded at 387 °C when the maximum degradation was ascertained. Consequently, it is noteworthy that the gas release process takes place in the temperature range of 250–550 °C. Moreover, it has to be mentioned that the C-O-C, C-C, C-OH, Si-C, or Si-O bond scission at 387 °C in the synthesized DS-PPD hybrid material took place. Moreover, the absorbance increase in the FT-IR spectrum may be due to some fragmentation–recombination reactions that occur at high temperatures. Generally speaking, both spectra show some other absorption bands of different intensities, corresponding to the gases released during the thermal degradation of the DS-PPD hybrid sample. However, there are main absorption bands, proving the chemical composition of hydrid material sourse, which are found to be as follows: 3738–3856 cm^{-1} is characteristic of stretching vibrations

of νOH; 1459–1518 cm^{-1} is characteristic of the in-plane deformation of δOH vibrations coming from H_2O molecules; 3616 cm^{-1} and 3677 cm^{-1} are characteristic of νNH_2 in an alchil–NH_2 bond, and the band at 857 cm^{-1} is characteristic of out-of-plane deformation vibrations (γNH_2) coming from amine fragments; the band at 1646 cm^{-1} is in aromatic hydrocarbons; the bands at 2357 cm^{-1} and 677 cm^{-1} are recorded for the stretching vibration νC = O in carbon dioxide and at 2109 cm^{-1} in carbon monoxide; the large band at 2874–3011 cm^{-1} is characteristic of the stretching vibrations of $\nu CH/\nu CH_2$, while in-plane deformation vibrations are found at 1411 cm^{-1} (δCH_2) and 1355 cm^{-1} (δCH) to be coming from aliphatic fragments; the bands at 2693 cm^{-1} (νCH) and 1740 cm^{-1} (νCO) come from stretching vibrations in aliphatic aldehyde; and the bands found at 1036 cm^{-1} (νC-O-C), 1123 cm^{-1} (νSi-O-Si), 1258 cm^{-1} ($\nu Si-CH_3$), and 2179 cm^{-1} (νSi-H) are characteristic of stretching vibrations in aliphatic ethers and siloxane derivatives. All the components of the gas emissions were identified according to the IR spectra available in the literature reports and the NIST library [24–26].

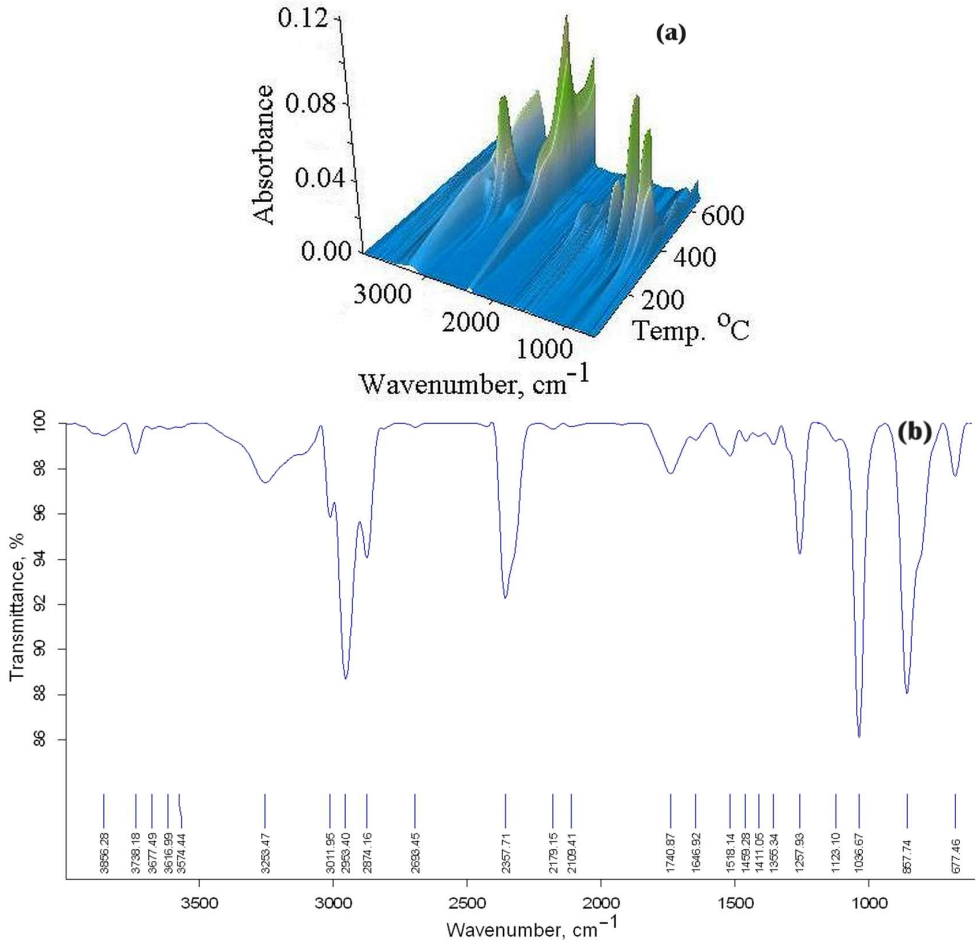

Figure 5. (**a**) The temperature-dependent FT-IR 3D spectrum of a DS-PPD (1/0.5) solid sample and (**b**) the FT-IR spectrum of gasses evolved during the thermal degradation of the DS-PPD (1/0.5) sample recorded at 387 °C.

Thereafter, to confirm the data obtained from the FT-IR analysis, the gas emission composition was evaluated based on the MS spectrum. Thus, the temperature at which the gas composition was identified was the temperature (390 °C) at which the maximum quantity of released gas was achieved, as determined from Gram–Schmidt curves using Proteus software (Table 1). Therefore, in Figure 6, the MS spectrum shows many mass-to-charge (m/z) signals, which are assigned to molecular and ionic fragments, coming out of the thermal decomposition of the DS-PPD hybrid siloxane material. Moroever, it

is observed that most of the m/z units are lower than 100, with peak intensities directly reflecting ionic species' abundance. The MS spectrum allowed us to determine the chemical structures of the resulting products of the thermal degradation of the DS-PPD siloxane hybrid sample based on the molecular weights of the ionic fragments identified.

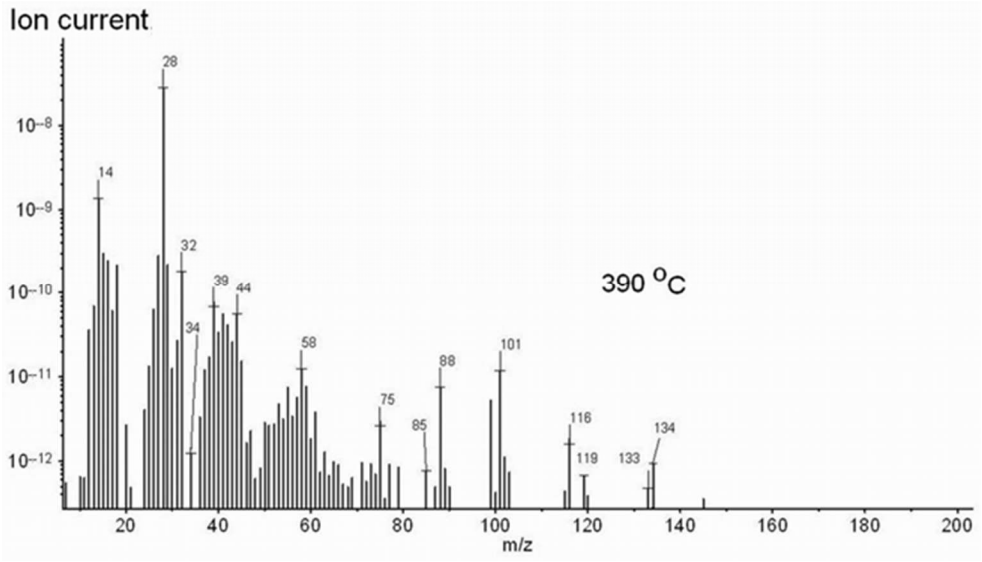

Figure 6. MS spectrum of thermal degradation products recorded at 390 °C min^{-1} (at the maximum temperature of evolved gases) for the DS-PPD hybrid sample.

Thus, according to the NIST database, it was possible to assign the following chemical structures found in the gas emission: water (H_2O^+, m/z = 18, 17, 16); carbon dioxide (CO_2^+, m/z = 44, 28, 16, 12); carbon monoxide (CO^+, m/z = 28, 16, 12); aliphatic derivative as methane (CH_4^+, m/z = 16, 15, 14, 13, 12); ethane ($C_2H_6^+$, m/z = 30, 29, 28, 27, 26, 25, 15,); propane ($C_3H_8^+$, m/z = 44, 43, 41, 39, 29, 28, 27, 26,15); propanal ($C_3H_6O,^+$ m/z = 58, 57. 39, 29, 28, 27, 26); benzene ($C_6H_6^+$, m/z = 78, 79, 77, 74, 52, 51, 50, 49, 39, 38); propyl amine ($C_3H_9N^+$, m/z = 59, 41, 30, 28); methyl propyl ether ($C_4H_{10}O^+$, m/z = 74, 45, 41, 29, 27, 15); ethyl eter ($C_4H_{10}O^+$, m/z = 74, 59, 45, 31, 29, 28, 27, 15); 1,1,3,3-tetramethyl disiloxane ($C_4H_{14}OSi_2^+$, m/z = 134, 133, 120, 119, 103, 73, 59, 45); and dimethylethyl silane ($C_4H_{12}Si^+$, m/z = 88, 87, 73, 59, 58, 45, 43, 31, 29). The results derived from MS spectrometry are in good agreement with the obtained FT-IR data, and the presence of all found compounds is also confirmed by the literature data reported [27,28].

2.4. Wettability Study

The wettability levels of the gp-DS and PPD precursors and synthesized DS-PPD sample have been investigated by measuring the static contact angle (CA) of the two liquids, water (w) and ethylene glycol (eg), with the prepared hybrid solid surface. The calculated average values of the ten consecutive measurements of the contact angles are given in Table 2. For both measurements (w and eg), ten frames taken at various time intervals (0–0.15 s) were considered to be the mean CA for each case. In general, it is considered that a CAw value of 90 degrees is the border that separates a hydrophobic character from a hydrophilic character [29]. As we expected, gp-DS is hydrophobic when in contact with both liquids (this being a property of all siloxanes), while PPD is hydrophilic. In the DS-PPD sample, the CAs were found to be CAw = 97.0° and CAeg = 85.7°, respectively. Consequently, one may conclude that the prepared DS-PPD sample contains only a few polar groups on its surface, proving that it has a not-so-good surface wettability, conferring a dual weak hydrophilic/hydrophobic character on the hybrid siloxane material.

Table 2. CA_w and CA_{eg} for gp-DS, PPD, and DS-PPD.

Sample	CA_w [deg]	CA_{eg} [deg]	Standard Deviation [deg]
gp-DS	101.4	92.1	0.15–0.30
PPD	82.1	77.6	0.17–0.29
DS-PPD	97.0	85.7	0.16–0.32

2.5. Optical Properties Investigation

Because the material's optical properties are usually described by the magnitude of the band gap energy (E_g) [30], the UV-visible spectrum of the synthesized DS-PPD hybrid material has been recorded and is shown in Figure 7a. As observed, the maximum absorption at around 387 nm is indicative of an n−π* transition, coming from the unsaturated system of the PPD component [31]. This suggests an indirect transition between energy levels, further allowing us to draw the Tauc plot (Figure 7b) and estimate the band gap energy, 3.2 eV, for the obtained DS-PPD hybrid material via the extrapolation of the linear region of the spectrum to the energy axis. This finding recommends using the prepared DS-PPD hybrid siloxane material for UV-based applications.

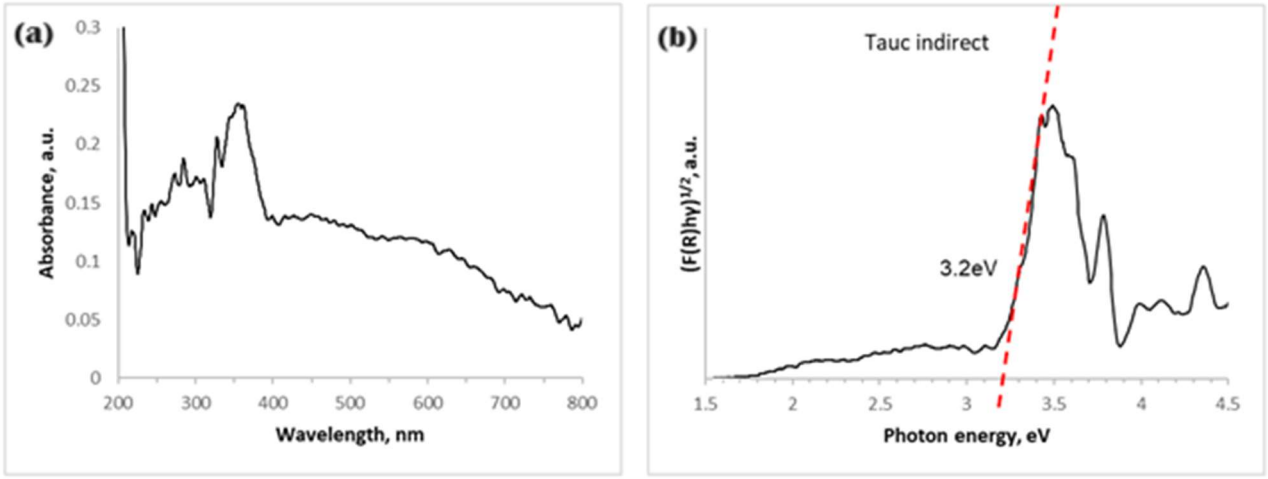

Figure 7. UV-Vis (DRS) absorption spectrum (**a**) and Tauc plot (**b**) of the synthesized DS-PPD hybrid siloxane material.

The evaluation of the band gap energy was carried out considering the diffuse reflectance spectrum of the as-synthesized DS-PPD sample (Figure 7b). The reflectance data were processed within the Tauc model equation, where the Kubelka–Munk function was introduced [32] as follows:

$$[F(R_\infty)E]^{1/n} = B(E - E_g) \quad (1)$$

where $F(R_\infty) = \frac{(1-R_\infty)}{R_\infty}$ is defined as the Kubelka–Munk function and $R = \frac{R_s}{R_{std}}$, where R_s and R_{std} are the reflectance values of the sample and standard, respectively; $E = h\nu$, E_g denotes the band gap energy; and n is a parameter that takes values depending on the type of transition. Usually, the calculation of Eg is performed by evaluating the linearity of the equation (1) for the two types of transitions: direct allowed transitions (n = ½) and indirect allowed transitions (n = 2). The plots of $[F(R_\infty)E]^{\frac{1}{n}}$ as a function of photon energy are displayed for the indirect allowed transitions in Figure 7b. The representation of Tauc equation modified with the Kubelka–Munk function reveals a band gap energy for the indirect allowed transition, which corresponds to n = 2.

3. Materials and Methods

3.1. Materials

1,1,3,3 tetramethyl disiloxane 97% (DS), allyl glycidyl ether 99% (AGE), Karstedt catalyst, chloroform, and p-phenylenediamine (PPD) were purchased from Sigma-Aldrich Chemie GmbH (Eschenstrasse 5, D-82024 Taufkirchen, Germany) and used as received. Toluene (Sigma-Aldrich Chemie GmbH Eschenstrasse 5, D-82024 Taufkirchen, Germany) was dried over sodium wire and distilled before use.

The synthesis of hybrid materials was performed via a two-step procedure. At the first stage, 1,1,3,3-tetramethyldisiloxane (DS) was first hydrosilated with allyl glycidyl ether (AGE) in the presence of a platinum catalyst. In the second step, the obtained glycidoxypropyl-disiloxane (gp-DS) was modified with paraphenylenediamine (PPD), and a new compound was obtained.

3.1.1. Synthesis of 1,3-bis(glycidoxypropyl)-1,1,3,3-tetramethyldisiloxane (gp-DS)

1,3-bis(glycidoxypropyl)-1,1,3,3-tetramethyldisiloxane (gp-DS) was prepared according to a previously reported procedure for the hydrosilation of AGE with DS in the presence of Karstedt catalyst in toluene [33].

^{1}H-NMR ($CDCl_3$); δ, ppm: 0.01–0.07 (Si–CH_3); 0.46–0.5 (Si–CH_2); 1.53–1.61 ($CH_2CH_2CH_2$); 2.57–2.78 (CH_2 of epoxy cycle); 3.01–3.14 (CH of epoxy cycle); and 3.35–3.695 (CH_2–O).

FT-IR (cm^{-1}): 2963, 2907, 2874 (CH vibrations of methyl and methylene groups), 1261, 843, 802 (Si-CH_3 vibrations), 1190 (C-O-C vibration), 1094, 1022 (Si-O-Si stretching), and 910 (epoxy-ring vibration) [22].

3.1.2. Synthesis of Disiloxane–Phenylenediamine Conjugate (DS-PPD)

1,3-bis(glycidyloxypropyl)-1,1,3,3-tetramethyldisiloxane (gp-DS) was mixed with p-phenylenediamine (PPD) at an equimolar ratio of epoxy groups to reactive hydrogen atoms from amine (epoxy/NH_2 = 1:0.5 molar ratio) in the presence of chloroform. The manipulation of reactants and the reaction itself were carried out under a dark and dry argon atmosphere. The resulting mixture was homogenized by using a mechanical stirrer and kept at 60 °C for 24 h. After the vacuum evaporation of chloroform, a brown solid was obtained. The product prepared was, thus, washed with ethyl alcohol to remove any excess PPD and separated via filtration, and the residual solvents were evaporated in a vacuum at 50 °C. The obtained product was not completely soluble, although several solvents and mixtures of solvents were used. The best solubilization was achieved in DMSO by stirring and heating for 24 h. The soluble part was 63.5%, and the insoluble part was 36.5%.

^{1}H-NMR soluble fraction, 400 MHz, $CDCl_3$) δ (ppm): 0.07 (12H, s, 4xCH_3-Si), 0.51–0.55 (4H, m, 2xCH_2-Si), 1.61–1.63 (4H, m, 2xCH_2-propyl), 3.44–3.47 (12H, m, 2xCH_2-O-CH_2 and 2xCH_2-N), 3.95–4.03 (2H, m, 2xCH(OH)), and 6.61–6.83 (4H, m, CH, PPD).

FT-IR (cm^{-1}): 3406, 3375 (N-H stretching); 3196 (C-C stretching); 3007 (C-H stretching); 1628 (C-N-H bending); 1516 and 1456 (C-C stretching); 1308 (C-N stretching); 1261 (C-N-C bending); 1126 and 1065 (C-H in-plane deformation); 829 (disubstituted aromatic ring); 798 (N-H bending); 719 (C-H out of plane bending); and 515 (C-C deformation) [22].

The simplified reaction of the epoxy by the amine is presented in Scheme 1.

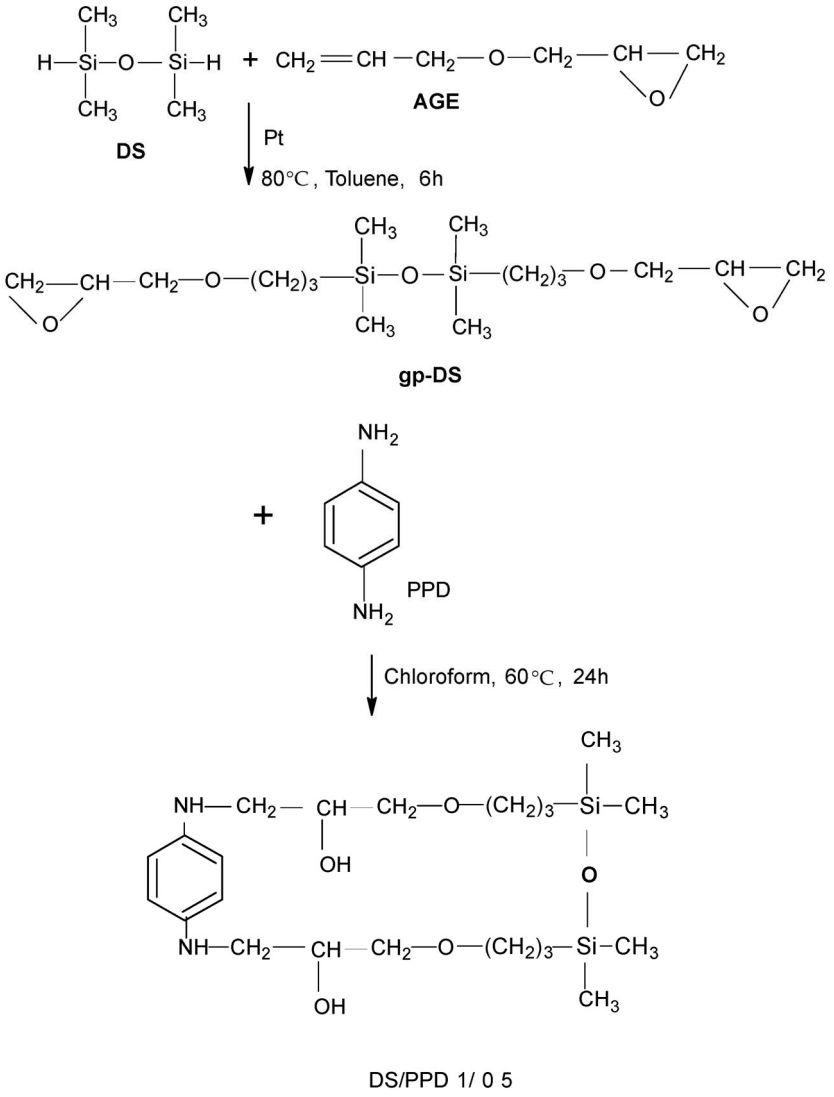

Scheme 1. Schematic representation of the synthesis reaction mechanism of DS-PPD (1/0.5) siloxane hybrid material.

3.2. Methods

FTIR spectra were recorded via a Thermo Fisher Scientific Nicolet 60 SX spectrometer (Thermo Fisher Scientific, Waltham, MA, USA), using KBr pellets, in the range of 4000–400 cm^{-1}.

The NMR spectra were recorded at room temperature using a Bruker Avance NEO 400 MHz spectrometer (Bruker Company, Billerica, MA, USA) equipped with a 5 mm inverse detection, z-gradient, multinuclear probe. $CDCl_3$ was used as a solvent for the NMR analysis, and the chemical shift values were referenced to the residual solvent signal (^{1}H $CDCl_3$: 7.26 ppm)

Mass spectrometry analysis was carried out using a Bruker UltrafleXtreme MALDI-TOF/TOF mass spectrometer (Bruker Company, Billerica, MA, USA) equipped with a nitrogen laser and operated in the positive ion mode.

The morphology and composition of samples were examined using a Quanta 200 scanning electron microscope (FEI Company, Hillsboro, OR, USA), operated with a beam voltage of 10 kV, and provided with an EDX elemental analysis system (Ametek, Berwyn, PA, USA).

Thermogravimetric analysis (TGA), coupled with FTIR spectroscopy measurements, was used for (i) the simulation/acceleration of thermal aging when conducted in the presence of oxygen, (ii) the evaluation of the thermal behavior of the material, and

(iii) the identification of decomposition products. Thus, the thermal characterization of the cured product and monomers was carried out using a STA 449 F1 Jupiter apparatus (Netzsch-Gerätebau GmbH, Wittelsbacherstraße, Selb, Germany) coupled to a Vertex 70 spectrophotometer (Bruker Company, Billerica, MA, USA) and Aeolos QMS 403C mass spectrometer (TG/DTA/FT-IR/MS) (Netzsch-Gerätebau GmbH, Wittelsbacherstraße, Selb, Germany) for the simultaneous characterization of the evolved gases. The samples with masses of up to 15 mg were placed in Al_2O_3 crucibles and degraded with a heating rate of 10 °C min^{-1} under a nitrogen atmosphere in the temperature range of 30–650 °C. Al_2O_3 was used as a reference material. The gases that resulted from thermal decomposition were transferred through a polytetrafluorethylene line with a 1.5 mm diameter and heated to 190 °C using an TGA-IR external modulus equipped with a MCT detector (Mercury Cadmium Telluride) (Thorlabs Inc., Newton, NJ, USA), which covers a spectral range from 600 to 4000 cm^{-1}. The IR signals were registered with OPUS 6.5 software in 3D size. The transfer line to QMS spectrometer was made of a quartz capillary, with a 75 µm diameter, and heated at 290 °C. The QMS spectrometer works under vacuum (10–5 mbar) and has an electron impact ionization energy of 70 eV. The MS data were recorded in the range of m/z = 1–200, and the processing of these data was accomplished using Aeolos 3.2 software.

X-ray diffraction analysis was performed using a Rigaku Miniflex 600 diffractometer (Applied Rigaku Technologies, Inc., Austin, TX, USA) using CuKα-emission in the angular range 2–90° (2θ), with a scanning step of 0.01° and a recording rate of 2°/min.

The wettability (hydrophobicity) of the DS-PPD hybrid was investigated by measuring the contact angle of a drop of liquid placed on the surface of the sample using the KSV Cam 200 device from KSV Instruments Ltd. (Helsinki, Finland). Two liquids with different physical properties (density and viscosity) were chosen—water (its density is 0.9986 g/cm^3 (~1); its viscosity is 25.5 mPa·s) and ethylene glycol (its density is 1.11 g/cm^3; its viscosity is 13.76 mPa·s)—to study the hydrophobicity of the composite under different conditions. Ten measurements were performed for each liquid guide drop.

UV-Vis (DRS) measurements were performed using a Shimadzu UV-2400 spectrophotometer (Shimadzu, Kyoto, Japan), equipped with an ISR-2200 integrating sphere, and by using MgO pellets as white standard.

4. Conclusions

Amine functional hybrid siloxane was synthesized via a coupling reaction between 1,3-bis(glycidoxypropyl) tetramethyldisiloxane and para-phenylenediamine. The obtained structure was proved by FTIR and ^{1}H-NMR spectroscopies, with the results revealing a successful epoxy–amine curing reaction. Then, the TG curves of PPD and gp-DS samples show a sudden and rapid product degradation, while the curve recorded on DS-PPD hybrid siloxane exhibits a wide thermal degradation process at higher temperatures accompanied by a lower degradation speed, achieving higher thermal stability than its precursors. Further, it was found that the DS-PPD hybrid siloxane surface behaves as a hydrophobic material in contact with water droplets (viscosity of 25.5 mPa·s and density of 1 g/cm^3) and a hydrophilic material in contact with ethylene glycol droplets (density of 1.11 g/cm^3 and viscosity of 13 mPa·s). Thus, the synthesized sample simultaneously exhibits both hydrophilic and hydrophobic properties. Regarding the optical properties of the DS-PPD hybrid material, indirect transitions between energy levels were found to occur, resulting in a band gap energy of 3.2 eV. This could serve as valuable information regarding the further application of the synthesized hybrid material in UV-based applications.

In conclusion, the siloxane hybrid material, the DS-PPD sample, has been successfully synthesized and characterized from structural, thermal, and morphological points of view. The main finding of the present study emphasizes the assessment of the thermal stability of the prepared hybrid paraphenylenediamine-siloxane material in terms of reactive epoxy and amino groups, coming from paraphenylenediamine, used as a curing agent, and 1,3-bis(3-glycidoxypropyl)-1,1,3,3-tetramethyldisiloxane.

Author Contributions: Conceptualization, M.E.F. and M.I.; methodology, N.T.; software, N.T. and E.U.; validation, V.H. and M.I.; formal analysis, R.R. and E.U.; investigation, M.E.F. and M.I.; resources, E.U.; data curation, M.I.; writing—original draft preparation, M.E.F.; writing—review and editing, M.I. and N.T.; visualization, M.I. and E.U.; supervision, V.H. All authors have read and agreed to the published version of the manuscript.

Funding: This study received no external funding.

Data Availability Statement: The original contributions presented in the study are included in the article, and are available upon request.

Conflicts of Interest: The authors declare no conflicts of interest.

References

1. Yilgör, E.; Yilgör, I. Silicone containing copolymers: Synthesis, properties and applications. *Prog. Polym. Sci.* **2014**, *39*, 1165–1195. [CrossRef]
2. Yi, B.; Wang, S.; Hou, C.; Huang, X.; Cui, J.; Yao, X. Dynamic Siloxane Materials: From Molecular Engineering to Emerging Applications. *Chem. Eng. J.* **2020**, *405*, 127023. [CrossRef]
3. Ratna, D. *Handbook of Thermoset Resins*; Smithers Rapra Technology: Billingham, UK, 2009.
4. Paluvai, N.R.; Mohanty, S.; Nay, S.K. Synthesis and Modifications of Epoxy Resins and Their Composites: A Review. *Polym. Plast. Technol. Eng.* **2014**, *53*, 1723–1758. [CrossRef]
5. Maity, T.; Samanta, B.C.; Dalai, S.; Banthia, A.K. Curing study of epoxy resin by new aromatic amine functional curing agents along with mechanical and thermal evaluation. *Mat. Sci. Eng. A* **2007**, *464*, 38–46. [CrossRef]
6. Ignatenko, V.Y.; Ilyin, S.O.; Kostyuk, A.V.; Bondarenko, G.N.; Antonov, S.V. Acceleration of epoxy resin curing by using a combination of aliphatic and aromatic amines. *Polym. Bull.* **2019**, *77*, 1519–1540. [CrossRef]
7. Fache, M.; Montérémal, C.; Boutevin, B.; Caillol, S. Amine hardeners and epoxy cross-linker from aromatic renewable resources. *Eur. Polym. J.* **2015**, *73*, 344–362. [CrossRef]
8. Savonnet, E.; Le Coz, C.; Grau, E.; Grelier, S.; Defoort, B.; Cramail, H. Divanillin-based aromatic amines: Synthesis and use as curing agents for fully vanillin-based epoxy thermosets. *Front. Chem.* **2019**, *7*, 606. [CrossRef]
9. Akbari, R.; Beheshty, M.H.; Shervin, M. Toughening of dicyandiamide-cured DGEBA based epoxy resins by CTBN liquid rubber. *Iran. Polym. J.* **2013**, *22*, 313–324. [CrossRef]
10. Ramos, V.D.; Costa, H.M.; Soares, V.L.P.; Nascimento, R.S.V. Modification of epoxy resin, a comparison of different types of elastomer. *Polym. Test.* **2005**, *24*, 387–394. [CrossRef]
11. Yeh, J.M.; Huang, H.Y.; Chen, C.L.; Su, W.F.; Yu, Y.H. Siloxane-modified epoxy resin–clay nanocomposite coatings with advanced anticorrosive properties prepared by a solution dispersion approach. *Surf. Coat. Technol.* **2006**, *200*, 2753–2763. [CrossRef]
12. Tao, Z.; Yang, S.; Chen, J.; Fan, L. Synthesis and characterization of imide ring and siloxane-containing cycloaliphatic epoxy resins. *Eur. Polym. J.* **2007**, *43*, 1470–1479. [CrossRef]
13. Murias, P.; Byczyński, Ł.; Maciejewski, H.; Galina, H. A quantitative approach to dynamic and isothermal curing of an epoxy res-in modified with oligomeric siloxanes. *J. Therm. Anal. Calorim.* **2015**, *122*, 215–226. [CrossRef]
14. Byczynski, Ł.; Dutkiewicz, M.; Maciejewski, H. Thermal and surface treated p-Phenylenediamine and p-Toluidine. *J. Environ. Anal. Toxicol.* **2015**, *5*, 1000329.
15. Chakraborty, R. Development of Novel Cycloaliphatic Siloxanes for Thermal and UV-Curable Applications. Master's Thesis, The Graduate Faculty of the University of Akron, Akron, OH, USA, 2008.
16. Rosu, D.; Mustateata, F.; Cascaval, C.N. Investigation of the curing reactions of some multifunctional epoxy resins using differential scanning calorimetry. *Thermochim. Acta* **2001**, *370*, 105–110. [CrossRef]
17. Innocenzi, P.; Kidchob, T. Hybrid organic-inorganic sol-gel materials based on epoxy-amine systems. *J. Solgel Sci. Technol.* **2005**, *35*, 225–235. [CrossRef]
18. Trivedi, M.K.; Branto, A.; Trivedi, D.; Nayak, G.; Singh, R.; Jana, S. Characterization of physical, thermal and spectroscopic properties of biofield energy properties of hybrid materials obtained from epoxy-functional urethane and siloxane. *Polym. Bull.* **2016**, *73*, 1247–1265.
19. Sanchez, C.; Julian, B.; Belleville, P.; Popall, M. Applications of hybrid organic–inorganic nanocomposites. *J. Mater. Chem.* **2005**, *15*, 3559–3592. [CrossRef]
20. Maciejewski, H.; Da bek, I.; Fiedorow, R.; Dutkiewicz, M.; Majchrzak, M. Thermal stability of hybrid materials based on epoxy functional (poly)siloxanes. *J. Therm. Anal. Calorim.* **2012**, *110*, 1415–1424. [CrossRef]
21. Harabagiu, V.; Pinteala, M.; Cotzur, C.; Holerca, M.N.; Ropot, M. Functional Polysiloxanes. Reaction of 1,3-bis(3-glycidoxypropyl)-1,1,3,3-tetramethyldisiloxane with amino compounds. *J. Macromolec. Sci. A* **1995**, *32*, 1641–1648. [CrossRef]
22. Savitskii, A.V.; Kuznetsov, L.M. Infrared spectrum of paraphenylenediamine dihydrochloride. *J. Struct. Chem.* **1971**, *12*, 1016–1018. [CrossRef]
23. Fortună, M.E.; Ignat, M.; Asandulesa, M.; Rotaru, R.; Pricop, L.; Harabagiu, V. Improved physico-chemical properties of mesoporous carbon by functionalization with aminopropyl-polydimethylsiloxane (APPDMS). *J. Inorg. Organomet. Polym. Mater.* **2018**, *28*, 2275–2287. [CrossRef]

24. Tudorachi, N.; Lipsa, R.; Mustata, F.R. Thermal degradation of carboxymethyl starch-g-poly(lactic acid) copolymer by TG-FTIR-MS analysis. *Ind. Eng. Chem. Res.* **2012**, *51*, 15537–15545. [CrossRef]
25. Kupareva, A.; Arvela, P.M.; Grénman, H.; Eränen, K.; Murzin, D.Y. Base-catalyzed transformations of tetramethyldisiloxane. *Ind. Eng. Chem. Res.* **2013**, *52*, 10080–10088. [CrossRef]
26. Godoy, N.V.; Segatelli, M.G. Kinetic investigation of thermal formation processes of SiOC glasses derived from C-containing hybrid polymeric networks. *J. Braz. Chem. Soc.* **2015**, *1*, 899–909. [CrossRef]
27. Tudorachi, N.; Chiriac, A.P.; Mustata, F. New nanocomposite based on poly(lactic-co-glycolic acid) copolymer and magnetite. *Synth. Charact. Compos. Part B* **2015**, *72*, 150–159. [CrossRef]
28. Mustata, F.; Tudorachi, N.; Asandulesa, M.; Bicu, I. Thermal and electrical behavior of hybrid thermosets based on epoxy and maleimide resins cured with p-aminobenzoic acid. *Int. J. Chem. Kinet.* **2019**, *51*, 799–814. [CrossRef]
29. Rotaru, R.; Fortuna, M.E.; Cojocaru, C.; Samoilă, P.; Pricop, L.; Harabagiu, V. Viscose-maghemite-goethite polymeric composite as sorbent for oil spill cleanup. *Environ. Eng. Manag. J.* **2019**, *18*, 1193–1200.
30. Callister, W.D., Jr.; Rethwisch, D.G. *Fundamentals of Materials Science and Engineering: An Integrated Approach*; John Wiley & Sons: Hoboken, NJ, USA, 2020.
31. Bistafa, C.; Modesto-Costa, L.; Canuto, S. A complete basis set study of the lowest n–π* and π–π* electronic transitions of acrolein in explicit water environment. *Theor. Chem. Acc.* **2016**, *135*, 129. [CrossRef]
32. Fifere, N.; Airinei, A.; Timpu, D.; Rotaru, A.; Sacarescu, L.; Ursu, L. New insights into structural and magnetic properties of Ce doped ZnO nanoparticles. *J. Alloys Compd.* **2018**, *757*, 60–69. [CrossRef]
33. Pricop, L.; Fortună, M.E.; Popovici, D.; Asandulesa, M.; Racles, C.; Zaltariov, M.F.; Marangoci, N.; Savin, M.; Harabagiu, V. Nickel Complexes of Guanidine Functionalized Trisiloxane. *J. Inorg. Organomet. Polym. Mater.* **2019**, *29*, 2024–2034. [CrossRef]